



# Statistical modeling of microstructurally short crack growth in high cycle fatigue

Mohammad Pourdavood<sup>\*</sup>, Philippe Bocher

École de Technologie Supérieure, Department of Mechanical Engineering, 1100 Notre-Dame, Montreal, H3C 1K3, Canada

## ARTICLE INFO

### Keywords:

Fatigue life dispersion  
Short crack growth  
High cycle fatigue  
Extreme value statistics  
Microstructural-sensitive modeling

## ABSTRACT

Capturing the behavior of short cracks under fatigue conditions has become a challenge for researchers. The early stage of crack propagation is influenced by microstructural features, such as grain boundaries and orientations, which leads to significant statistical variations. Models such as the ones developed by Navarro and De Los Rios have been able to describe the process by considering the average properties of the material and estimating the number of cycles related to the short crack stage. However, fatigue should be seen as an extreme value process. In the present work, a more realistic model was developed to consider the statistical nature related to grain orientations to estimate fatigue life dispersion. Eleven crack propagation criteria have been used to compute the number of cycles spent in the short crack stage. Parameters such as the Schmid factor, the potential crack length, and the various angles describing the misorientation between adjacent grains were considered. One thousand random scenarios for short crack growth were studied for each propagation criterion and some statistical analyzes were run to estimate the worst-case scenario out of one million. Results can be well described using the generalized extreme value distribution, capturing the stochastic nature of the fatigue life.

## 1. Introduction

Fatigue is a process inducing localized and permanent structural changes in materials subjected to varying loads. It may culminate in cracks that can grow and result in the complete fracture of the component after a certain number of these load variations, which for that reason is a topic of research in mechanical engineering [1]. Although fatigue process has been investigated for more than 150 years, it is still difficult to comprehend due to its statistical nature and many issues in this area still remain unsolved [2].

### 1.1. Crack growth stages

From an engineering perspective, fatigue crack growth in ductile metals has been classified into two stages: a microstructure-sensitive stage (called stage I) and a microstructure-independent stage (stage II) [3,4].

The first stage is responsible for a large portion of the fatigue life in mechanical components, even as much as 90 % in the high cycle fatigue (HCF) and very high cycle fatigue (VHCF) regimes [5–7]. It corresponds to two steps: crack nucleation and microstructurally short crack (MSC)

propagation. MSC refers to crack size of the same magnitude as the average microstructure (generally, less than 10 times of the grain diameter) [3,8]. MSC growth typically includes acceleration and deceleration until the crack reaches the second stage [9–11].

The first step of the stage I is the nucleation of a crack, or more specifically in the context of the present article, the apparition of a physical discontinuity inside a grain. Fatigue cracks are formed from the accumulation of localized plastic deformation due to load fluctuations. This localized plasticity can be due to the presence of actual stress raisers in the material (pores or inclusions), or due to some specific configurations of the grain orientation and grain's neighborhood that introduce elastic and plastic stress transfers [12,13]. In most cases, dislocations slip on favorably oriented planes leads to the development of persistent slip bands (PSBs), which evolve into fatigue cracks due to damage accumulation [14]. Although crack initiation is a relevant step of the fatigue process as it may significantly contribute to the total number of fatigue cycles, it was not considered in the present work.

The second step of stage I corresponds to the propagation of MSC to the next grains. The size of the plastic zone ahead of the crack is of the same order as microstructure and the crack, and plastic damage accumulation in this zone plays a significant role in the propagation process [15–20]. In this step, crack propagation behavior is highly influenced by

<sup>\*</sup> Corresponding author.

E-mail addresses: [Mohammad.pourdavood.1@ens.etsmtl.ca](mailto:Mohammad.pourdavood.1@ens.etsmtl.ca) (M. Pourdavood), [Philippe.Bocher@etsmtl.ca](mailto:Philippe.Bocher@etsmtl.ca) (P. Bocher).

**Nomenclature:**

$a$	crack length
$b$	the magnitude of the Burgers vector
$c$	plastic zone size
$da/dN$	crack growth rate
$D_{mean}$	average grain diameter
$f$	fraction of dislocations participating in crack growth
$g$	grain number
$G$	shear modulus
$i$	number of half grains that the plastic zone covers
$k$	angle between two slip directions of two grains
$K$	stress intensity factor
$L$	unit vector of loading direction
$m_g$	orientation factor of grain $g$
$m'_g$	Wilkinson's orientation factor of grain $g$
$n$	crack to plastic zone size ratio
$n_c$	critical crack to plastic zone size ratio
$n_s$	initial crack to plastic zone size ratio
$N_{MSC}$	loading cycles for microstructurally short crack propagation
$N_p$	unit vector of normal to the slip plane
$N_q$	unit vector of the slip direction
$SF_g$	Schmid factor of grain $g$
$\alpha$	angle between two normal vector of the two slip plains
$\beta$	tilt angle
$\Delta N_g$	loading cycles for crack propagation through grain $g$
$\Delta\sigma$	macroscopic applied stress range
$\sigma$	maximum applied stress

$\sigma_{comp}$	comparison stress
$\sigma_f$	friction stress
$\sigma_{FL}$	fatigue limit
$\sigma_{L_g}$	local critical stress
$\sigma_y$	yield stress
$\sigma_U$	ultimate strength
$b$	scale parameter
$\xi$	shape parameter
$\mu$	location parameter
$\varphi$	angles between the traces of slip plane and load axis on the sample surface
$\psi$	twist angle
$\nu$	Poisson's ratio
$\omega$	angles between the traces of slip plane and load axis on the grain boundary plane
$\emptyset$	crack tip displacement

**Abbreviations**

FCGR	Fatigue Crack Growth Rate
GB	Grain Boundary
GC	Geometrical Compatibility
GEV	Generalized Extreme Value
HCF	High Cycle Fatigue
LCF	Low Cycle Fatigue
MSC	Microstructurally Short Crack
N-R	Navarro and De Los Rios
OP	Optimization Parameter
PSB	Persistent Slip Band
VHCF	Very High Cycle Fatigue

microstructural features, such as grain boundaries (GBs) and grain orientation. These features affect dislocation motion ahead of the crack tip, which leads to MSC deflection, deceleration, and acceleration [18–20]. In the present work, only the statistical contribution related to the MSC propagation in the HCF and VHCF regimes was investigated (typically for more than  $10^6$  or  $10^8$  cycles, respectively).

Analyzing of fatigue cracks has shown deflection during MSC propagation relating to the crack passage through GBs. Gao et al. [21] have studied the effect of GBs on MSC's behavior in a nickel-base superalloy René 104 - ME. They reported that MSCs were deflected at GBs, with a correlation between the magnitude of GB misorientation and crack deflection, the higher the misorientation the larger the deflection. Chen et al. [10] provide very clear examples of cracks changing directions whenever they pass through a GB in an AA2524-T3 Aluminum alloy under HCF regime. They show that slip planes with high applied shear stress (high Schmid factors) were selected for crack growth. Yan et al. [22] have also shown that in a 2524-T3 aluminum alloy, MSCs grow with numerous path changes and they tend to propagate on planes with high Schmid factors.

These changes in directions along the path are associated with significant fluctuations in terms of crack growth [23]. It was found experimentally that whenever the tip of a propagating crack gets close to a GB, the fatigue crack growth rate (FCGR) decreases [9,10,21,24], and the crack may even stop for a large number of cycles or even stop and never propagate again, preventing the crack to reach the stage II. If stress concentration ahead of the crack tip is high enough to generate some plasticity in the next grain after some fluctuation, the crack will propagate into the next grain, resulting in a significant increase in the crack growth rate. Ma et al. [24] have studied the MSC behavior of Inconel 718 alloy by using in-situ SEM and reported substantial FCGR fluctuations during fatigue tests that decelerations correlated with the presence of GB ahead of the crack tip and accelerations when the crack

entered in a new grain.

**1.2. Modeling MSC propagation**

Many models have been proposed to describe the fatigue crack behavior during MSC propagation [25–27]. In these models, the equations from LEFM are modified even if LEFM is limited to long crack [28]. In 1963, the Bilby-Cottrell-Swinden (BCS) model [29] employed the continuously distributed dislocation theory to quantify slip activities in the plastic zone ahead of a crack tip. In this model, the material was idealized homogenous and dislocation motion was described using the macroscopic theory of plasticity. In 1988, Navarro and De Los Rios (N-R) [9] introduced in the BCS model some crystallographic considerations and the concept of microstructural barriers proposed ten years earlier by Taira et al. [15].

The 1D model proposed by N-R estimates the number of cycles that is representative of the MSC growth stage. Five main hypotheses can be found as the bases for their theoretical development. Firstly, all grains have the same size corresponding to the average grain diameter of the material. Secondly, short crack propagates straightly; in particular, there is no deflection during short crack growth. Thirdly, the region that undergoes plasticity at the crack tip stays inside the grain in which the crack is propagating: the concept is that the plastic zone gets blocked by the GB until dislocation sources in the next grain reach to a critical value, allowing the next grain to undergo plastic deformation. Fourthly, the amount of applied stress required to activate dislocation sources in the next grain decreases as the crack grows through more grains. In the latter version of their model [18], they introduced a fifth hypothesis to introduce the effect of grain orientations: they assumed that as the crack size increases, the grains orientation is statistically less favorable for short crack propagation.

Despite its simplicity, the N-R model was capable of predicting some

facts about the propagation of MSC. The model has been used to predict the fatigue life of a mild carbon steel on five different applied stress ranges and the results compared well with experiments with 10 %–26 % errors [9]. Hussain et al. [30] have conducted fatigue test on C-Mn steel for seven different applied stress ranges and compared with the N-R model, which shows errors of 2 %–22 % with experiments when the N-R model was used for predicting the stage I. Pannemaecker et al. [31] have used the N-R model to simulate fretting fatigue on 7050-T7451 aluminum alloy reaching a good agreement with experimental results (relative error less than 5 %).

Some modified versions of the N-R model were proposed recently. Koltz et al. [32] have introduced residual stress and cold work profile in the model to quantify the effect of shot peening on the fatigue life of Inconel 718 samples. The effect of residual stress was included through crack closure stress and cold work profile considered by using a finite element model. The model, used in the HCF and low cycle fatigue (LCF) regimes, was capable of predicting the average fatigue life with a 15 % error. Wei et al. [33] have also proposed a conjunction of the N-R model with the Newman's crack closure model on Al 7010-T7451 samples tested under random and constant amplitude loading. The results show an average difference between experimental data and predicted fatigue life of 7.5 % for constant amplitude conditions and 14 % for random loading conditions.

The present approach proposes to modify the N-R model to tackle the variability in fatigue performance for different initial microstructures and propagation hypotheses. The N-R model will be explained in detail in order to justify and specify the additions proposed in the present model in order to take into consideration local properties of the microstructure. The number of cycles obtained for various propagation criteria and microstructures will be analyzed using extreme value statistics as fatigue is an extreme values process. In fact, the fastest crack that reaches to the long crack propagation stage controls the fatigue life of mechanical components.

## 2. Methodology

### 2.1. Navarro and De Los Rios formalism

The N-R model considers each side of the crack independently and the crack growth rate for one side is defined as  $da/dN$ . It is considered proportional to the plastic displacement at the crack tip  $\varnothing$  as in Eq. (1) [9].

$$\frac{da}{dN} = f\varnothing \quad (1)$$

where  $f$  is the fraction of dislocations on the slip band participating in the process of crack propagation. The plastic displacement at the crack tip  $\varnothing$  can be estimated by Eq. (2) as proposed in Ref. [26]. It is equal to the number of dislocations that are present in the plastic zone multiplied by the Burgers vector  $b$ .

$$\varnothing = \frac{2b}{A\pi^2} \sqrt{c} \left[ 2\sigma_f \sqrt{c} n \ln\left(\frac{1}{n}\right) + K\sqrt{\pi(1-n^2)} \right] \quad (2)$$

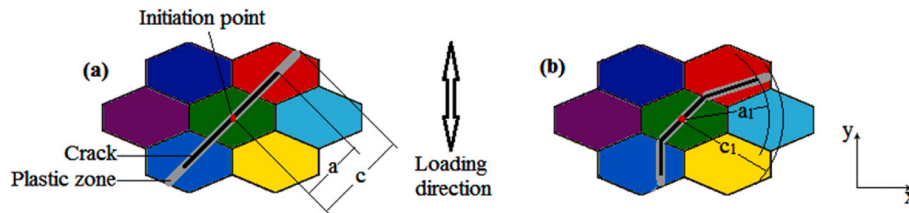


Fig. 1. Schematic representation of MSC propagation illustrating the crack size  $a$  and plastic zone size  $c$ : a) the N-R model b) present model. The loading direction and X-Y axis are added.

here  $\sigma_f$  is the friction stress,  $K$  is the stress intensity factor, and  $A$  is a constant that describes the nature of the dislocations taken into consideration ( $A = Gb/2\pi$  for screw dislocations and  $A = Gb/2\pi(1-\nu)$  for edge dislocations, where  $G$  and  $\nu$  are shear modulus and Poisson's ratio, respectively).

Finally,  $n$  plays a significant role in the model as it quantifies the difference between the crack size  $a$  and the size of the region that has undergone plastic deformation  $c$ .  $n$  is defined as the ratio between these two sizes as in Eq. (3) and Fig. 1(a).

$$n = a/c \quad (3)$$

A consequence of the model proposed by N-R is that the transition between the plastic and the elastic regions ahead of the crack is located at the GB. In other words, the plastic zone of a crack that newly penetrated in a grain reaches instantaneously to the next GB and stays there until the dislocation sources of the next grain get activated. Thus,  $c$  which is equal to the crack size  $a$  plus the size of the plastic region ahead of the crack tip is also equal to the distance between the center of the initial crack and the next GB. The position of the plastic region can then be referred to by an odd number of half grains  $i$  ( $=1, 3, 5$ , etc.) while the grains along the crack path are referred to by the number  $g = (i + 1)/2$ . Because the crack can propagate in zigzag in the new developed model, the plastic zone size is not necessarily an equal to an integer number of half-grain diameter as shown in Fig. 1(b).

Based on N-R third hypothesis, the crack in grain  $g$  can propagate into the next grain ( $g+1$ ) when the stress ahead of the plastic zone activates dislocation sources in the next grain [26]. If the applied stress fluctuations  $\Delta\sigma$  are constant, the stress concentration ahead of the plastic zone is controlled by the relative position of the crack tip blocked at the GB. The size of the crack increases with each fluctuation, and so does the value of parameter  $n$ . Increasing  $a$  and  $n$ , result in an increase in the stress concentration ahead of the plastic zone, and the process continues until it reaches the critical value that will activate plasticity in the next grain. This happens when  $n$  equals a critical value  $n_c$  that represents the adequate condition to activate dislocation sources in the next grain. The value of  $n_c$  for the GB  $g$  is estimated using Eq. (4):

$$n_{c_g} = \cos \left[ \frac{\pi}{2} \left( \frac{\sigma - \sigma_{L_g}}{\sigma_{comp}} \right) \right] \quad (4)$$

where  $\sigma_{comp}$  is a material parameter called comparison stress that corresponds to the stress that captures the resistance to plastic deformation at the crack tip, and  $\sigma_{L_g}$  is the local critical stress needed for the crack to go through the GB  $g$ . Accordingly, the higher the local critical stress  $\sigma_{L_g}$ , the higher the value of  $n_c$  and the closer the crack tip should get to the GB before dislocation sources could be activated in the next grain. Consequently, a higher number of fluctuations is required for crack to go through the next grain.

When grain  $g + 1$  starts to undergo plastic deformation, the frontier between the plastic and the elastic regions moves to the next GB and the value of  $n$  decreases suddenly to  $n_s$ , giving the opportunity for the crack to propagate further at the next cycle. Based on BCS's equation, N-R have estimated  $n_s$  for the grain  $g + 1$  as in Eq. (5) and the number of cycles required for crack propagation through grain  $g$ ,  $\Delta N_g$ , can be

computed using Eq. (6):

$$n_{s_{g+1}} = n_{c_g} \frac{i}{i+2} = n_{c_g} \frac{2g-1}{2g+1} \quad (5)$$

$$\Delta N_g = \frac{G}{f(1-\nu)\Delta\sigma} [\sin^{-1}(n_{c_g}) - \sin^{-1}(n_{s_g})] \quad (6)$$

where  $f$  is the fraction of dislocations contributing to slip band formation already introduced in Eq. (1).

The stress components  $\sigma_{comp}$  and  $\sigma_{L_g}$  in Eq. (4) are parameters that have to be determined for a given material. Making a strong assumption, N-R [26] assumed that  $\sigma_{comp}$  is equal to the ultimate tensile strength of the material, saying that it represents well the cyclic flow stress near the crack tip. On the other hand, they have defined  $\sigma_{L_g}$  from the fatigue limit of the material  $\sigma_{FL}$  as proposed in Eq. (7):

$$\sigma_{L_g} = \frac{m_g}{m_1} \frac{\sigma_{FL}}{\sqrt{\frac{c}{D_{mean}/2}}} \quad (7)$$

The ratio  $m_g / m_1$  was introduced to take into consideration grain misorientation and  $D_{mean}$  stands for the average grain diameter. Based on this equation, the local critical stress for the first grain is equal to the fatigue limit of the material.

The term  $m$  is used as an orientation factor equivalent to the inverse of Schmid factor: having a minimum value when the grain is favorably oriented for dislocation glide. In the N-R model, the first grain  $m_1$  has the minimum value since crack initiation takes place on a plane with maximum resolved shear stress. They consider that statistically the longer is the crack the less favorably oriented is the next grains for crack propagation and the orientation factor. The orientation term of the grain  $g$ ,  $m_g$ , is then expected to systematically increase with the grain number  $g$  and two equations have been proposed by N-R to estimate the value of the grain orientation ratio [18,20]:

$$\frac{m_g}{m_1} = 1 + 0.5 \ln(i) \quad (i = 1, 3, 5, \dots) \quad (8)$$

$$\frac{m_g}{m_1} = 1 + 2.07 \left[ \frac{2}{\pi} \arctan(s(i-1)) \right]^t \quad (i = 1, 3, 5, \dots) \quad (9)$$

where  $s$  and  $t$  in Eq. (9) are constants chosen in Ref. [20], equal to 0.522 and 1.86, respectively. The orientation ratio, equal to 1 in the first grain, increases slowly with  $i$  when using Eq. (8), whereas it increases rapidly using Eq. (9) with an asymptotic behavior toward 3.07 for FCC material (equivalent to the Taylor factor [20]).

The second part of Eq. (7) decreases as the crack size increases. It relates the macroscopic fatigue limit of the material  $\sigma_{FL}$  to the actual relative size of the plastic zone  $c$ . The size of the microstructure is taken into consideration thanks to the square root of the ratio between the plastic zone size and the mean grain radius ( $D_{mean} / 2$ ).

With these proposed parameters, the N-R model predicts that crack will slow down at GBs but it cannot predict that short crack may stop before reaching the stage II of crack propagation stage. Crack can stop at GBs only if the local critical stress related to the GB retardation,  $\sigma_{L_g}$ , can increase with  $i$ ; but, according to Eqs. (8) and (9) with the parameters proposed by N-R, the number of cycles needed for crack to growth through the next grains can only decrease as crack propagates. Although the first part of Eq. (7) increases continuously, the second part decreases at a higher rate resulting in decreasing values of  $\sigma_{L_g}$ , a lower  $n_c$  through Eq. (4), and eventually the crack does not need to stop at the GB to activate the dislocation sources in the next grain. Consequently, the difference between  $n_s$  and  $n_c$  decreases and the related number of cycles too (Eq. (6)).

## 2.2. Other considerations on MSC propagation

Wilkinson in Ref. [34] has proposed a methodology to estimate the orientation factor by defining  $m'_g$  as the minimization of the inverse dot product (noted “.”) of the normal to each slip plane ( $N_p$ ) with the unit vector of the load direction ( $L$ ) multiplied by the dot product of the associated slip directions ( $N_q$ ) with the same unit vector ( $L$ ) as expressed in Eq. (10). This is actually equivalent to the inverse of the maximum Schmid factor found in the crystal.

$$m'_g = \min_{p,q} \left( \frac{1}{(L \cdot N_p)(L \cdot N_q)} \right) = \frac{1}{\max(SF_g)} \quad (10)$$

Unlike in Eqs. (8) and (9), this orientation factor,  $m'_g$ , is not forced to increase monotonically as the crack grows; instead, its value can increase or decrease according to the orientation of the grains. In the present work, a formulation using the Schmid factor will be rather used as in Eq. (11):

$$\frac{m_g}{m_1} = \frac{0.5}{SF_g} \quad (11)$$

where,  $SF$  is the Schmid factor of the slip system on which the crack is propagating (grain  $g$ ) or the Schmid factor of the potential slip system for crack propagation in the grain  $g+1$ , depending on which criteria is chosen.

When considering the propagation of a crack between one grain to the next, twist ( $\psi$ ) and tilt ( $\beta$ ) angles can be used to define the misorientation between the considered slip planes. The twist and tilt angles are defined as the angles between traces of two slip planes on the GB plane and on the plane that is perpendicular to the GB plane, respectively. Concretely, it is hard to fully describe the interaction between two slip systems since a three-dimensional description of the GB position is needed [35–37]. Zhai et al. [27] simplified the situation considering the GB perpendicular to the observation surface and parallel to the load axis. Considering Zhai methodology, tilt angle can be defined as the angle between traces of two slip planes on the sample surface. A schematic representation of the twist and tilt angles are provided in Fig. 2. In this condition, twist and tilt angles can be computed using angles between the traces of slip plane and load axis on the GB plane ( $\omega$ ), the gray plane in Fig. 2, and sample surface ( $\varphi$ ), the X-Y plane, as expressed in Eqs. (12) and (13), respectively [27].

$$\psi = |\omega_1 - \omega_2| \quad (12)$$

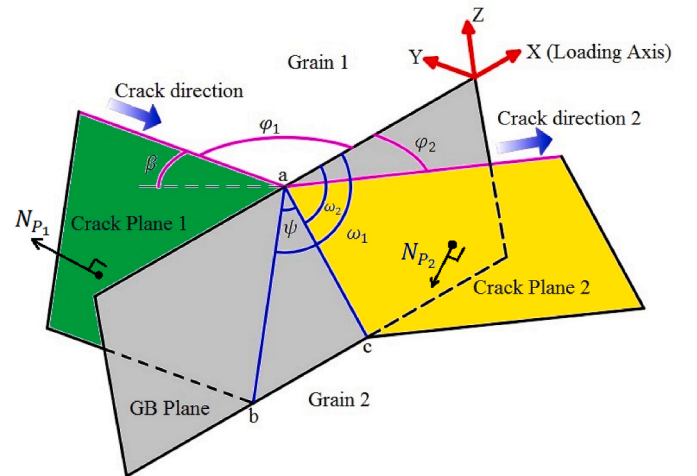


Fig. 2. Representation of the twist ( $\psi$ ) and tilt ( $\beta$ ) angles and the geometrical implication that can explain misorientation between two grains.

$$\beta = |\varphi_1 - \varphi_2| \quad (13)$$

The tilt angle ( $\beta$ ) is an important parameter having effect on short fatigue crack behavior. It contributes to the resistance of a GB against crack propagation through the next grain by decreasing the fatigue driving force at the crack tip. Small tilt angles maintain high fatigue driving force for short crack propagation. In most cases, slip planes that offer small twist and tilt angles are favorable for short fatigue crack propagation [27]. In the present work, the tilt angle is considered as one of the parameters that capture the effect of grain misorientation on crack behavior.

Luster et al. [38] suggested a geometrical compatibility ( $GC$ ) factor that only relates to the slip misalignment between the two grains without considering the effect of the GB plane. Two angles were considered: the angle  $k$  between the two slip directions and the angle  $\alpha$  between the two normal to the slip planes. This geometrical compatibility factor is calculated as in Eq. (14).

$$GC = \cos(k)\cos(\alpha) \quad (14)$$

When the  $GC$  factor is maximized, the geometrical compatibility is high and the transition from one grain to the next is geometrically compatible. This factor does not consider the orientation of the GB plane, but is a convenient approximation suitable for 2-D simulations. The angle  $\alpha$  is the second parameter used in the present model to find impact of the grain orientation on the MSC growth, which is calculated as in Eq. (15).

$$\alpha = \arccos\left(\frac{N_{P_1} \cdot N_{P_2}}{|N_{P_1}| |N_{P_2}|}\right) \quad (15)$$

where  $N_{P_1}$  and  $N_{P_2}$  are the vectors of the normal of the two favored slip planes in the neighboring grains, as shown in Fig. 2.

### 2.3. The presented model for MSC propagation

In order to document the statistical effect of crystal orientations on MSC propagation, 2-D polycrystalline aggregates have been generated. A hexagonal grid  $17 \times 17$  with a total of 289 cells is considered. A grain is defined at the center of this structure and eight rows of grains around it build the possible environment for MSC propagation. In the present version of the model, only the effect of grain orientations has been considered; in particular, a distribution of grain sizes was not considered and all grains have the same size and an equiaxed shape. As in the N-R model, the stress at the grain level is considered equivalent to the macroscopic stress and no stress transfer from the neighboring grains were taken into consideration. Furthermore, the contribution of defects, including inclusions, on crack nucleation and MSC propagation was not considered. Random orientations were assigned to all the grains, except the central grain for which orientation maximizing the Schmid factor (0.5) was chosen. By construction, a fatigue crack is put at the center of the central grain on the slip system that maximizes shear stress. One thousand sets of grain were thus generated, providing one thousand possible scenarios on which various MSC propagation models can be run.

If the N-R model is a 1-D model, the present version proposes an extension to a 2-D one. In the present version, grains have the same geometry assumed to be the average grain size of the material (as in the N-R model), However, the actual available slip distance is considered in the model introducing a variability in the propagation path. In addition, only the surface propagation of the MSC is considered, ignoring for the moment the fact that MSC also propagate under the surface, i.e., inside the material. However, it is relevant to note that MSCs do propagate extensively on the surface, conversely to long cracks that propagate more easily inside the material due the triaxiality effect (crack propagate faster in plain strain condition). As for the 1-D N-R model, these assumptions do not prevent tackling certain key effects of the microstructure on fatigue crack propagation. The main goal of the present

work is to develop N-R model one step further, and capture the stochastic nature of the fatigue life. Future version of the model, based on cellular automaton principal, will be able to extend the model to more complex representations of the microstructure.

All criteria for crack growth in the stage I include selection of the slip system on which the crack will propagate in the next grain and the calculation of the number of cycles required to pass the GB. Five optimization parameters (OP) have been considered to select the slip system on which the crack could grow in the next grain, each one minimizing the propagation energy. In addition, three methods were used to estimate the number of cycles required to pass the GB, each one considering different equation to calculate  $\sigma_{L_g}$ .

In the developed model, selection of the slip system for crack propagation is based on OP. The first OP is related to the Schmid factor of the next grain: crack will propagate on the slip system having the highest Schmid factor. For the second and third OPs, crack propagates to the slip system that maximizes  $\cos(\alpha)$  and  $\cos(\beta)$ , respectively. This is tied to the preference of the crack to choose a slip system in the next grain in a way that minimizes its deflection, i.e., minimizing the energy required to activate crack nucleation sites in the new grain. The fourth OP is based on the first three OPs, calculated as the maximization of the product of these three OPs, which means that crack propagates through slip system having high Schmid factor, not necessarily the highest, and at the same time it does not require high deflection at GB. The last OP introduces a geometrical parameter related to the potential crack size ( $r$ ) on the selected slip plane, capturing the fact that crack tends to propagate on the slip plane on which more dislocations can pill up (reducing the local yield strength).

The number of cycles required to pass the GB is calculated through the estimation of  $\sigma_{L_g}$ . The properties of the grains encountered on the crack path being available, they can be used to calculate  $\sigma_{L_g}$ . The first method is the one proposed by N-R using Eq. (7) with the actual grain orientations instead of the average one (criterion 0). Here, the maximum Schmid factor of the grain that crack tip is located at the moment is chosen to calculate the value of  $\sigma_{L_g}$ ,  $\left(m_g/m_1 = 0.5/\max(SF_g)\right)$ . In the second method, the value of  $\sigma_{L_g}$  is computed by choosing the Schmid factor of the active slip system of the grain in which the crack tip is present (Eq. (16)). For the last method of  $\sigma_{L_g}$  calculation, the Schmid factor of the potential slip system in the next grain is chosen. This is motivated by the fact that activation of mobile dislocation in the next grain will cancel the microstructural barrier produced by the GB. However, there are several slip systems that can act as a source of mobile dislocations in the next grain, providing twelve possible values for  $\sigma_{L_g}$  as proposed in Eq. (17) (where  $j$  stand for one of these slip systems).

$$\sigma_{L_g} = \frac{0.5}{SF_g} * \frac{\sigma_{FL}}{\sqrt{\frac{2c_g}{D_{mean}}}} \quad (16)$$

$$\sigma_{L_{g,j}} = \frac{0.5}{SF_{(g+1)_j}} \frac{\sigma_{FL}}{\sqrt{\frac{2c_g}{D_{mean}}}} \quad (17)$$

here  $c_g$  is the length of the plastic zone from the center of the grain in which the crack has nucleated as illustrated in Fig. 1(b).

A total of eleven crack propagation criteria are considered, based on the selection of slip system for crack propagation (choosing one of the five OPs) and calculating  $\sigma_{L_g}$  (employing one of the three aforementioned methods), as summarized in Table 1. In the criterion 0, the first OP has chosen and  $\sigma_{L_g}$  is calculated by the first method mentioned above (Eq. (7)). It should be noted that crack path is forced to be straight in this criterion. In criteria 1 to 5, the second method is employed to estimate  $\sigma_{L_g}$  (Eq. (16)) and all five OPs are considered one by one (OP 1 for criterion 1, OP 2 for criterion 2, etc.). For criteria 6 to 10, the calculation of  $\sigma_{L_g}$  is based on the third method, incorporating each of the five OPs

**Table 1**  
Crack propagation criteria and their reference number.

$\sigma_{L_z}$	OP				
	$SF_{g+1}$	$\cos(\alpha)$	$\cos(\beta)$	$SF_{g+1} * \cos(\alpha) * \cos(\beta)$	$SF_{g+1} * \cos(\alpha) * \cos(\beta) * r$
Eq. (7)	0	-	-	-	-
Eq. (16)	1	2	3	4	5
Eq. (17)	6	7	8	9	10

individually (OP 1 for criterion 6, OP 2 for criterion 7, etc.). In Criteria 1 to 10, crack growth being constrained to specific active slip systems, it propagates in zigzag and its length plus the plastic zone ahead of the crack tip is not anymore equal to an integer number of half-grain

diameters. For each criterion, one thousand crack propagation scenarios are considered.

The algorithm built to estimates the number of cycles spent in the MSC propagation regime ( $N_{MSC}$ ) is illustrated in Fig. 3(b) and detailed

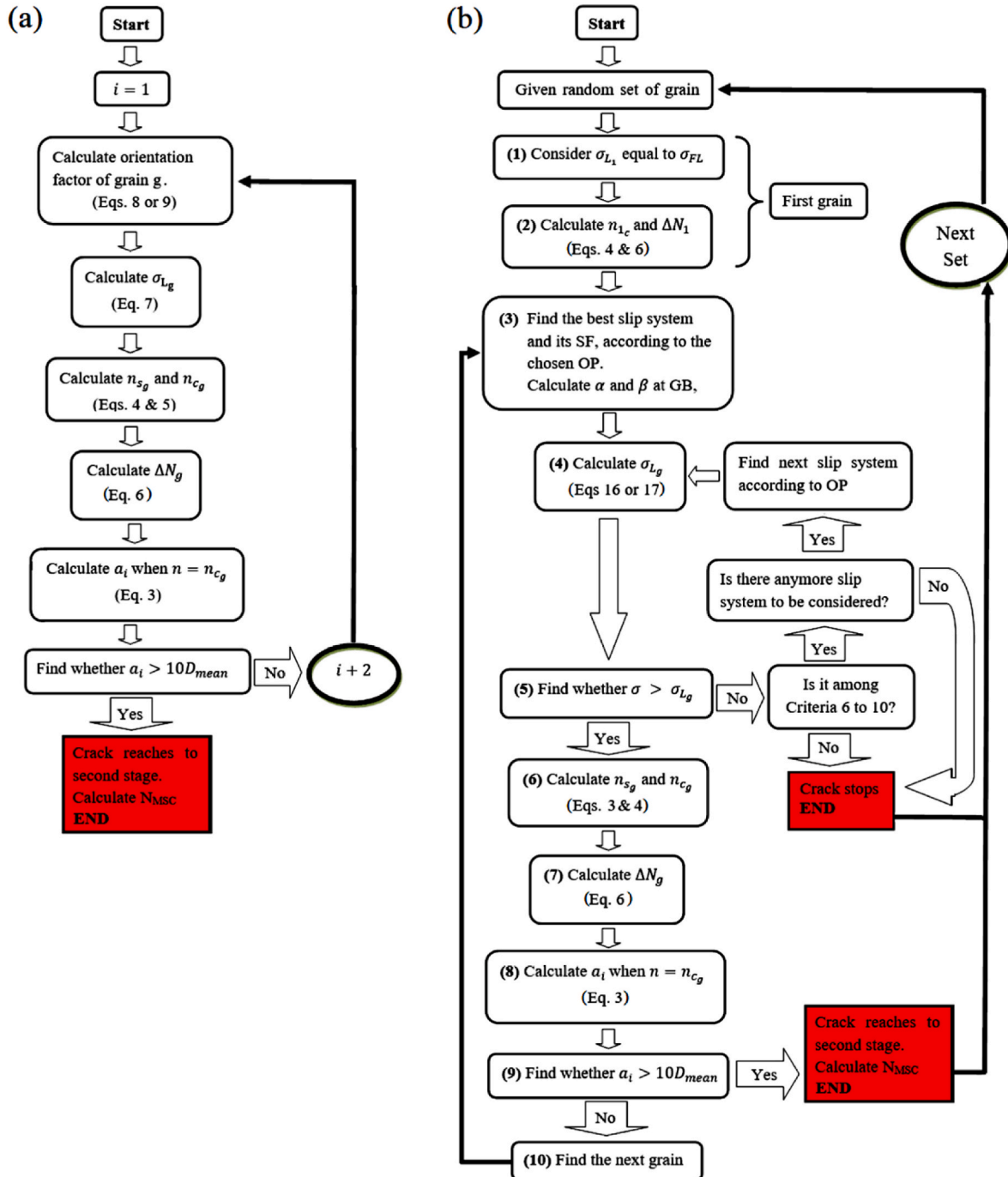


Fig. 3. Algorithm describing the a) N-R model and b) present model.

below. To clarify the difference between the two models, the algorithm used by N-R is shown in Fig. 3(a). In the present model, a 10-step process is run for the eleven criteria presented above, with one thousand generated microstructures for each criterion. The algorithm was programmed using Matlab R2017b and run on a personal computer equipped with Intel(R) xeon(R) CPU E3-1225 v6 @ 3.3 GHz. The calculation time for one thousand scenarios of a given propagation criterion takes less than 15 min.

The model estimates the behavior of the first (central) grain in the first two steps. Due to construction of the aggregate, the crack appears on a plane that maximizes the Schmid factor, i.e. at 45° from the loading direction. The number of cycles required to onset the crack nucleation is not taken into consideration by the present model, but the number of cycles required to move the nucleated crack to the next grain is. The value of local critical stress ( $\sigma_{L_i}$ ) for the first GB was considered to be equal to the fatigue limit of the material ( $\sigma_{FL}$ ) as in the N-R model. The value of parameter  $n_{c_i}$  and the number of cycles for crack propagation through the first grain is calculated by Eqs. (4) and (6), respectively, as step 2 in Fig. 3(a).

Based on the OP considered in the propagation criteria, the slip system  $j$  with the highest OP value in the next grain is selected in step 3 and  $\sigma_{L_{g_j}}$  calculated in step 4. If the obtained value is lower than the applied macroscopic stress, the value of parameter  $n_{c_g}$  and the number of cycles spent for passing over the GB ( $\Delta N_g$ ) is calculated using Eqs. (4) and (6), respectively, as steps 6 and 7 in Fig. 3(b). On the other hand, if the value of  $\sigma_{L_{g_j}}$  is larger than the applied stress, the crack will not be able to cross the GB and propagate on the plane containing the selected slip system. In this case, for criteria 1 to 5, crack will stop at that GB and will not go through stage II, since the value of  $\sigma_{L_{g_j}}$  depends on the active slip system of grain  $g$  and slip system of next grain has no effect on  $\sigma_{L_{g_j}}$ . On the other hand, for criteria 6 to 10, the next slip system that maximize the OP will be selected as a potential candidate and the associated  $\sigma_{L_{g_j}}$ , for that slip system will be calculated and compared with applied macroscopic stress. This process continues until considering all slip systems to find the favorable one for crack propagation. If all of the possibilities led to unfavorable condition for propagation, the crack will stop and will never reach the stage II.

The number of cycles ( $\Delta N_g$ ) spent to pass the GB  $g$  are calculated from  $\sigma_{L_{g_j}}$  using the parameter  $n_{c_g}$  and  $n_{s_g}$  for each grain on the crack path in step 7 from Eq. (6). Both sides of the crack are calculated independently, but the total crack size, which is considered as the summation of crack sizes on each side, is used to decide when the MSC enters in the stage II in order to stop the calculation (step 9 in Fig. 3(b)). It is set for a total crack size superior to 10 times the average grain diameter. The calculation is then stop, and the MSC propagation regime ( $N_{MSC}$ ) is calculated as the highest summation of the ( $\Delta N_g$ ) on each side of the crack.

It is relevant to note here that the orientation considered by the N-R equations is the grain in which the crack tip is, not the one in which the crack may propagate next (even though their propagation criterion is based on the propensity for the next grain to undergo plastic deformation). This consideration is not critical in the context of the N-R model as they are using average trends to describe material behavior, but it will be adapted in the present model to describe better the MSC behavior.

Furthermore, N-R considered the average properties of the microstructure, such as grain size and orientation factor, and consequently, it is the average behavior of the MSCs that is calculated and not the worst-case scenario. In reality, the fatigue performance is related to the worst-case scenario and failure will happen when most of MSCs have not yet reached stage II. It is actually the behavior of the MCSs nucleated in favorably oriented grains clusters that control the fatigue performance, and the associated probability of occurrence. In the proposed model, the orientation of each individual grain will be considered, allowing various situations to be explored.

## 2.4. Statistical analysis

One thousand sets of grains were generated to analyze statistically MSC propagation. Since the risk associated with the lowest number of cycles in the MSC propagation regime is considered as the most relevant parameter controlling the fatigue life of real parts, the data were analyzed using some extreme values statistics, the bloc minima method. The results of each criterion has been divided into 18 blocks. In each block, the lowest cycles was considered for analyzing with the GEV distribution. The Anderson-Darling test [39] was used to quantify the fitness of the model and the coefficients  $h$  and  $p$  were calculated to determine the goodness of fit (the closer  $h$  to 0 and  $p$  to 1, the better the fit). Tello et al. [40] proposed that  $p$ -value equal or lower than 0.05 is a strong evidence that the null hypothesis is rejected and so that the model cannot fit the results well.

The Generalized Extreme Value (GEV) distribution ( $G$ ) used to describe the maxima or minima of a large set of independent variables [41] was used to analyze the obtained data. In particular, it can be used to estimate the probability of a failure for a given number of cycles,  $N$ , with:

$$G(N) = \exp\left(-\left(1 + \xi \frac{(N - \mu)}{b}\right)^{\frac{1}{\xi}}\right) \quad (18)$$

where  $\xi$ ,  $\mu$  and  $b$  are shape, location, and scale parameters, respectively. The shape parameter defines the type of distribution: if  $\xi = 0$ , it is Gumbel type, for  $\xi > 0$  a Fréchet type, and for  $\xi < 0$  a Weibull type. The advantage of the GEV distribution is that the distribution type is specified by the analyzes of the data through the optimal shape parameter capable of fitting the data and the user does not require to assume which distribution should be used [42].

## 2.5. Material properties

The model in this paper was developed using Inconel 718 material data, which before machining, the material was forged and underwent solution treatment and aging to reach an average grain diameter of 25  $\mu\text{m}$  ( $D_{mean} = 25\mu\text{m}$ ). The Inconel 718 exhibited a random texture due to the recrystallisation process, leading to the formation of growth twins that randomize the grain orientation. The mechanical properties of the material are listed in Table 2. Fatigue tests for determining the  $\sigma_{FL}$  were run using 4 point rotating bending test ( $R = -1$ ) on a mirror polished surface ( $Ra < 0.1\mu\text{m}$ ) and a value of 448 MPa was found for  $10^6$  cycles [43]. In the present model, a fully reversed loading condition with the mean stress equal to 0 was considered, and the calculations were run slightly above the fatigue limit for a macroscopic applied stress  $\sigma$  of 450 MPa. In this paper, the term ‘‘applied stress’’ refers to the maximum stress applied in the fatigue process. The predicted results of the new model are compared with the results obtained from the N-R model.

## 3. Results and discussion

The number of cycles required for crack propagation in the second step of the stage I calculated for the N-R model and the new model, all based on actual grain orientations encountered in the microstructure are shown and discussed below. Even if it is the statistics related to the lowest number of cycles that are relevant as they will control the fatigue life of a component, it is relevant to compare the percentage of MSC reaching the stage II for each criterion. Because of the proposed parameters in the N-R model, all cracks reached to the stage II for criterion

**Table 2**  
Mechanical properties of studied Inconel 718.

Material	$\sigma_y$	$\sigma_U$ (MPa)	$\sigma_{FL}$ (MPa)	$G$ (GPa)	$\nu$
Inconel 718	1170	1363	448	77.2	0.29

0. In the other models, there is the possibility for some cracks to get arrested permanently on both sides of the crack, leading to a non-propagating condition. A large variation is found from a criterion to the next as displayed in Fig. 4: most of the MSCs reach the stage II for criterion 10 (up to 71 %), whereas only a few reach that stage for criterion 2 with 7 %.

The numbers of cracks reaching to the large crack growth stage are systematically lower for criteria 1 to 5 than their corresponding criteria 6 to 10. This could be explained by the fact that for criteria 1 to 5 there is only one slip system considered for the calculation of  $\sigma_{L_g}$ , reducing the possibility for the crack to find a propagation plane. For criteria 6 to 10, twelve slip systems are candidates in the next grain, providing that many chances to find a  $\sigma_{L_g}$  lower than the macroscopic applied stress (Eq. (17)). Criterion 2 and its corresponding criterion 7 have the lowest percentage of cracks reaching the stage II for their category, showing that if the  $\alpha$  angle plays a significant role, a large number of MSC will not reach the stage II of-crack propagation stage. Criteria 5 and 10 have the highest number of cracks reaching the stage II, suggesting that these crack propagation criteria give many options for a MSC to propagate. These criteria tend to favor long crack path, decreasing the value of  $\sigma_{L_g}$  (Eq. (16) and (17)) and allowing the crack to propagate to the next grain.

In terms of the number of cycles, the different criteria give surprisingly similar average behavior, similar to the one estimated by the classical N-R model that considers average behavior in terms of grain size and grain orientation, i.e. 569,310 cycles. The average, the first and third quartiles, minimum and maximum numbers for each criterion has shown in Fig. 5. By introducing the actual grain orientations in the N-R model (criterion 0), a lower average number of cycles at 520,153 is obtained with a low standard deviation. This low variation in term of cycles shows that the variation of maximum Schmid factors from one grain to the next does not introduce significant delays in the propagation behavior. Larger dispersions were found for the other criteria and the minimum number of cycles calculated for the thousand scenarios vary significantly from one to the next.

Even if proper statistical analysis will be run later in this paper, it is relevant to look at the critical paths associated with the lowest numbers of cycles found in the simulation as they would be the ones leading to failure. Illustrations are given in Fig. 6, where the colors represent the intensity of the Schmid factors in the aggregate. The numbers of cycles required for the crack to propagate through each grain are also reported for both sides of the crack. By construction, the initial crack, marked with the cyan color, is at  $45^\circ$  with respect to the loading direction and in the observation plane. Even in these fast-growing conditions, a large variety of crack path is found. Most of the grains on the critical paths have a rather large Schmid factors and at least one side of the crack is composed of grains only high Schmid factors: it is the side controlling the transition from MSC to large crack. Choosing high Schmid factor paths is more tangible for criteria 1 and 6 as in addition to  $\sigma_{L_g}$ , the OP

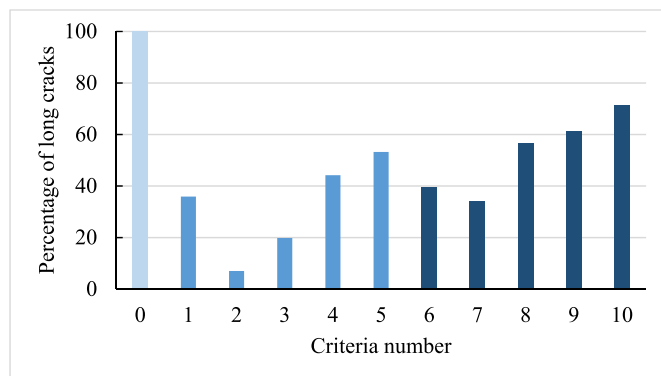


Fig. 4. Percentage of cracks reaching stage II for each criterion for 1000 random generated cases.

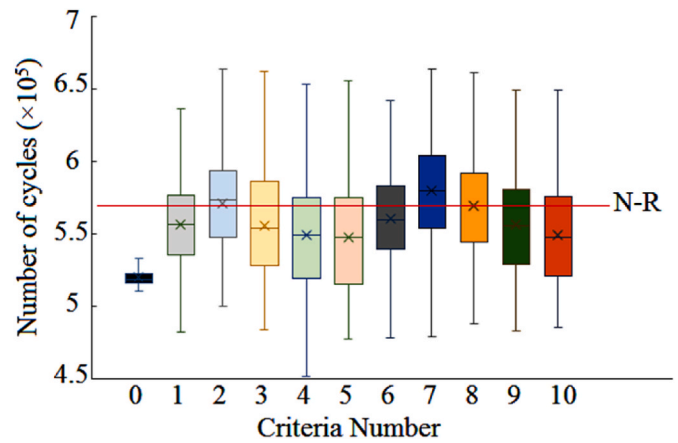


Fig. 5. Number of cycles spent in the MSC propagation regime for all criteria and reference N-R model (horizontal line). The moustache boxes represent the average, the first and third quartiles, minimum and maximum numbers.

depends on the Schmid factor of the grain. Interestingly, in criterion 2 the crack was able to propagate through the third grain on the left even if its Schmid factor is low at 0.30 since it is the Schmid factor of the grain that crack tip is located at the moment that defines the propagation criteria (the second grain having a Schmid factor of 0.48). The number of cycles needed for crack propagation through third grain (92,102) was more than the number of cycles for the second grain (85,524), since  $\sigma_{L_2} < \sigma_{L_3}$  even if the number of half grain has increased. In criterion 5, the same justification can be used to explain the propagation through the fourth grain on the left side (white arrow).

For criteria 6 to 10, the value of local critical stress depends on the Schmid factor of the next grain and examples of increasing numbers of cycles along the propagation path can be found even for the fastest cracks. In criterion 8, this number of cycles increase from grain 3 (62,291) to grain 4 (63,849) on the right side and similar values is reported for criterion 9 with grain 5 (35,601) and 6 (37,096) on the left side. Crack stops in the MSC regime after the fourth grains in criterion 10 on the right side due to a low value Schmid factor of the grain ahead (black arrow) but on the other side, grains are oriented favorably for fast crack propagation and low deflections at GBs.

The crack path of the critical condition is not simple and propagation direction changes at GB. The amount of deflection depends on the chosen slip system for crack propagation through the next grain, as OPs play an important role here. In criterion 2, crack path has changed significantly between grains 4 and 5 on the left side (black arrow) since the proposed OP is independent of  $\beta$  angle. Only low deflections are found when the OP depends on the  $\beta$  angle (criteria 3 and 8). Finally, the critical crack of criterion 10 shows a severe deviation between second and third grain on the right side, since OP depended significantly on the crack size and tend to select long propagating path (see the black arrow).

The 10 fastest scenarios for each criterion were analyzed and some statistics were obtained in terms of Schmid factors and GB's  $\alpha$  and  $\beta$  angles. The average, first and third quartiles, minimum and maximum values are presented in Fig. 7(a), (b) and (c), respectively. For criterion 0, a large Schmid factors ( $>0.42$ ), random  $\alpha$  and  $\beta$  angles are found with an average close to  $40^\circ$ . For most of the scenarios, crack propagates through slip system having high Schmid factors since the number of cycles to pass through a GB is related to  $\sigma_{L_g}$  which depended on this parameter. Most of the time, when OPs are only dependent on one parameter, the range of that parameter is limited: In criteria 1 and 6, Schmid factors are all higher than 0.4, the range of  $\alpha$  angles is small for criteria 2 and 7 with only a few degrees. It is also the case  $\beta$  angles for criterion 3, but not for criteria 8 (see Fig. 7(c)) for which the critical  $\beta$  angles along the crack path was spread between 2 and  $40^\circ$ , most of the GBs reported along the crack path were lower than  $8^\circ$  and just a few of

g	$\Delta N_g (\times 10^4)$		Schmid factor scale					$\Delta N_g (\times 10^4)$		g							
	Left	Right						Left	Right								
			Max	0.33	0.379	0.419	0.459				0.499						
			Min	0.33	0.38	0.42	0.46										
2	9.11	9.26	(1) $N_{MSC} = 4.82 \times 10^5$						(6) $4.78 \times 10^5$						8.67	8.74	2
3	6.81	6.41											6.09	6.68	3		
4	5.15	5.37											5.48	5.01	4		
5	4.27	4.03											4.14	4.24	5		
6	3.14	3.81											3.94	3.80	6		
2	8.55	9.02	(2) $5.01 \times 10^5$						(7) $4.79 \times 10^5$						8.66	8.92	2
3	9.21	6.99											8.77	7.6	3		
4	4.65	4.21											4.21	4.02	4		
5	4.01	4.02											3.71	3.42	5		
6	4.33	3.14											3.15	3.72	6		
2	10.50	8.74	(3) $4.84 \times 10^5$						(8) $4.86 \times 10^5$						8.94	9.15	2
3	7.41	6.55											6.72	6.23	3		
4	4.06	4.23											5.21	6.38	4		
5	4.18	3.86											3.69	3.86	5		
6	3.01	3.11											3.54	3.68	6		
2	8.97	8.64	(4) $4.52 \times 10^5$						(9) $4.82 \times 10^5$						8.91	9.51	2
3	6.61	5.98											5.88	6.54	3		
4	4.36	5.04											4.71	4.58	4		
5	3.51	3.21											3.56	4.64	5		
6	3.34	3.03											3.71	3.63	6		
2	10.20	9.96	(5) $4.78 \times 10^5$						(10) $4.85 \times 10^5$						8.72	8.79	2
3	6.64	6.88											5.79	9.71	3		
4	7.28	5.29											5.73	Stop	4		
5	4.38	5.01											4.18		5		
											3.47		6				
											2.29		7				

Fig. 6. Schematic representation of the critical path for the 10 models, Schmid intensity and the number of cycles for crack propagation in each grain for the worst-case scenario (critical path).

them were higher than  $22^\circ$ . These exceptions were found on the side that was not driving the fast growth of the MSC. The range of Schmid factor,  $\alpha$  and  $\beta$  angles are wider for criteria number 4, 5, 9 and 10 since it is a combination of these four parameters that are considered for finding the best slip system, reducing the dependency of one OP.

When a single parameter (OP 1 to 3) is used, the selected the slip system for crack growth are often not realistic. For instance, in the case of OP 1 (criteria 1 and 6), the propagating slip systems may have a high Schmid factor, but the  $\alpha$  and  $\beta$  angles may get notably high (see Fig. 7(b) and (c)), resulting into severe crack deflection at GBs. Multiple

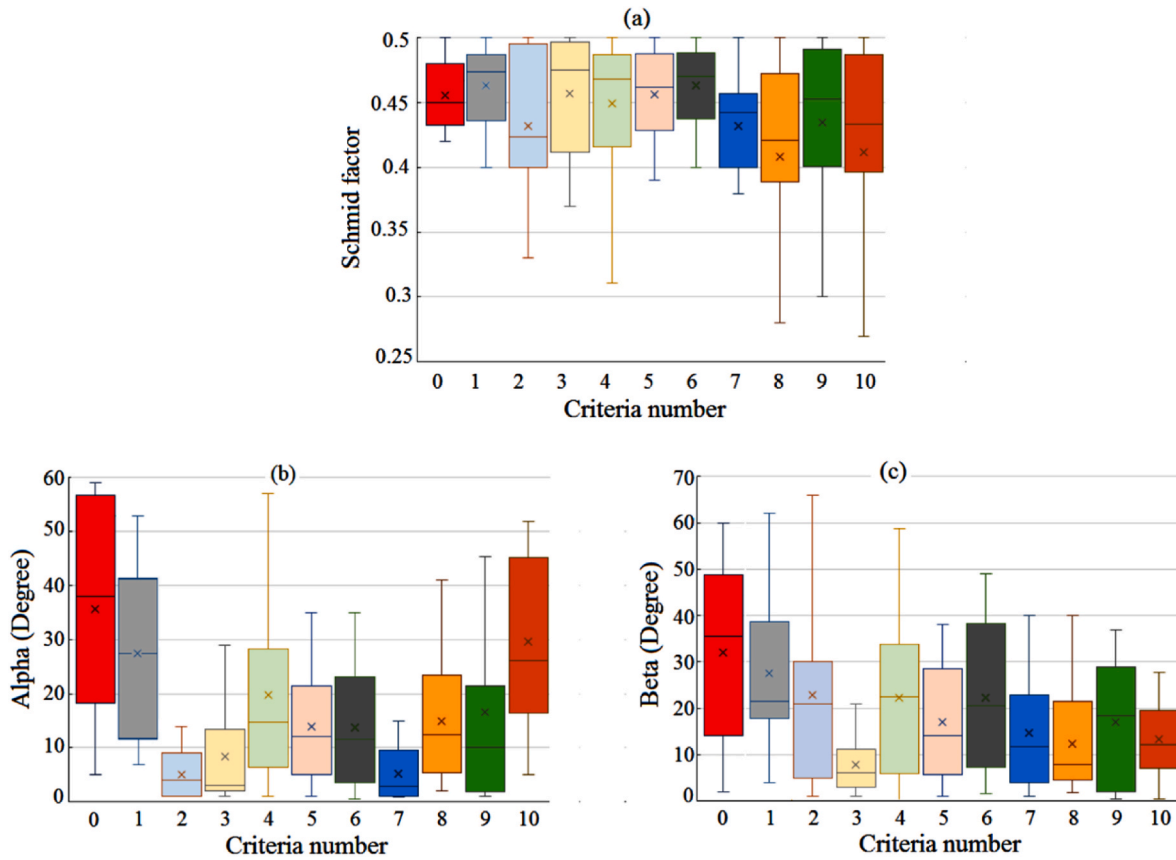


Fig. 7. Values of a) Schmid factors, b)  $\alpha$  and c)  $\beta$  angles of the grains on the propagation path for the 10 fastest cracks in the 11 criteria under investigation. The mustache boxes represent the average, the first and third quartiles, minimum and maximum values.

parameter criteria propose more realistic configurations. In OP 4 (criteria 4 and 9), for example, crack propagated through slip systems where the Schmid factor is high but not necessarily the highest available, while preventing severe deflections at GB. As a result, this approach provides a more accurate representation of experimental observations.

In the present model, crack can stop in one side but continue to propagate on the other. Two examples of these cracks have been selected and detailed in Fig. 8. Three approaches were considered to represent the effect of grain orientation with Eqs. (8), (9) and (11).

The value of grain orientation factor increases continuously with the grain number for both of N-R approaches (blue and red lines in Fig. 8(b) and (e)). As a result, when a crack propagates through the second grain, it will not stop. On the contrary, within Eq. (11), the grain orientation factor has the potential to either increase or decrease as the crack progresses through the adjacent grains (cyan and green lines in Fig. 8(b) and (e)), thereby potentially leading to crack arrest. For example, Fig. 8(a) shows a crack that arrested at the third GB since the value of grain orientation factor increased significantly. Another example has shown in Fig. 8(d), which grain orientation factor increased dramatically in the right side since the crack reached to a grain with low Schmid factor resulting in crack arrest.

The effect of the plastic zone size on the value of local critical stress ( $\sigma_{Lg}$ ) is quantified by the factor  $\frac{m_g}{m_1} \frac{1}{\sqrt{\frac{b}{\sigma}}}$ . If this factor is above 1, the crack will stop propagating as for the third GB on the right in Fig. 8(c) since the value of  $\frac{m_g}{m_1} \frac{1}{\sqrt{\frac{b}{\sigma}}}$  is equal to 1.3. The same condition has seen for the crack propagation through the second grain on the right in Fig. 8(f). It should be noted that as a crack grows, the influence of grain orientation on crack retardation decreases due to the decrease in the value of  $\frac{1}{\sqrt{\frac{b}{\sigma}}}$  leading to crack propagation even in low Schmid factor grains. For

instance, in Fig. 8(a), although crack reached to a grain with low Schmid factor (fourth grain left side), it has not stopped since the plastic zone size got big enough to overcome the unfavorable grain orientation. The same condition happened for the fifth grain on the left side of crack in Fig. 8(d).

As the fastest propagating cracks are extreme values in term of statistics, the results were further analyzed using the GEV distribution based on block minima approach considering 56 random simulations as a block. The shape ( $\xi$ ), location ( $\mu$ ) and scale ( $b$ ) parameters obtained for the 11 criteria are presented in Table 3. The values of the Anderson ( $h$ ) and Darling ( $p$ ) tests were calculated to test the possibility to use such a model to fit the obtained results. The values of  $h$  for all criteria were equal to zero and the  $p$  value bigger than 0.6, meaning that the GEV distribution is able to fit quite adequately the data set. The last column of Table 3 estimates the expected lowest number of cycles out of  $10^6$  scenarios based on the obtained GEV distributions.

The shape, location, and scale parameters can be compared for all criteria. For criterion 0, equivalent to the N-R model, the shape parameter  $\xi$  is negative meaning that the distribution can be described with Weibull and a small-scale parameter  $b$  of 677 was found. Except for criteria 1 and 10 for which Fréchet types were found, Weibull distributions were obtained for all criteria with much higher scale parameters than criterion 0: Criteria 10 and 2 having the lowest and highest scale parameters with values of 3162 and 24405, meaning they have the lowest and the highest dispersion among all criteria, respectively.

The location parameters  $\mu$  are not significantly different, from 482,116 cycles for criterion 4 to 529,101 for criterion 2, representing only a difference of about 9%. The location parameter of criteria 6, 8, 9 and 10 were slightly higher than their corresponding criteria (1, 3, 4, and 5), which indicates their distribution is shifted to the right meaning higher performance. In fact, considering 12 options for crack

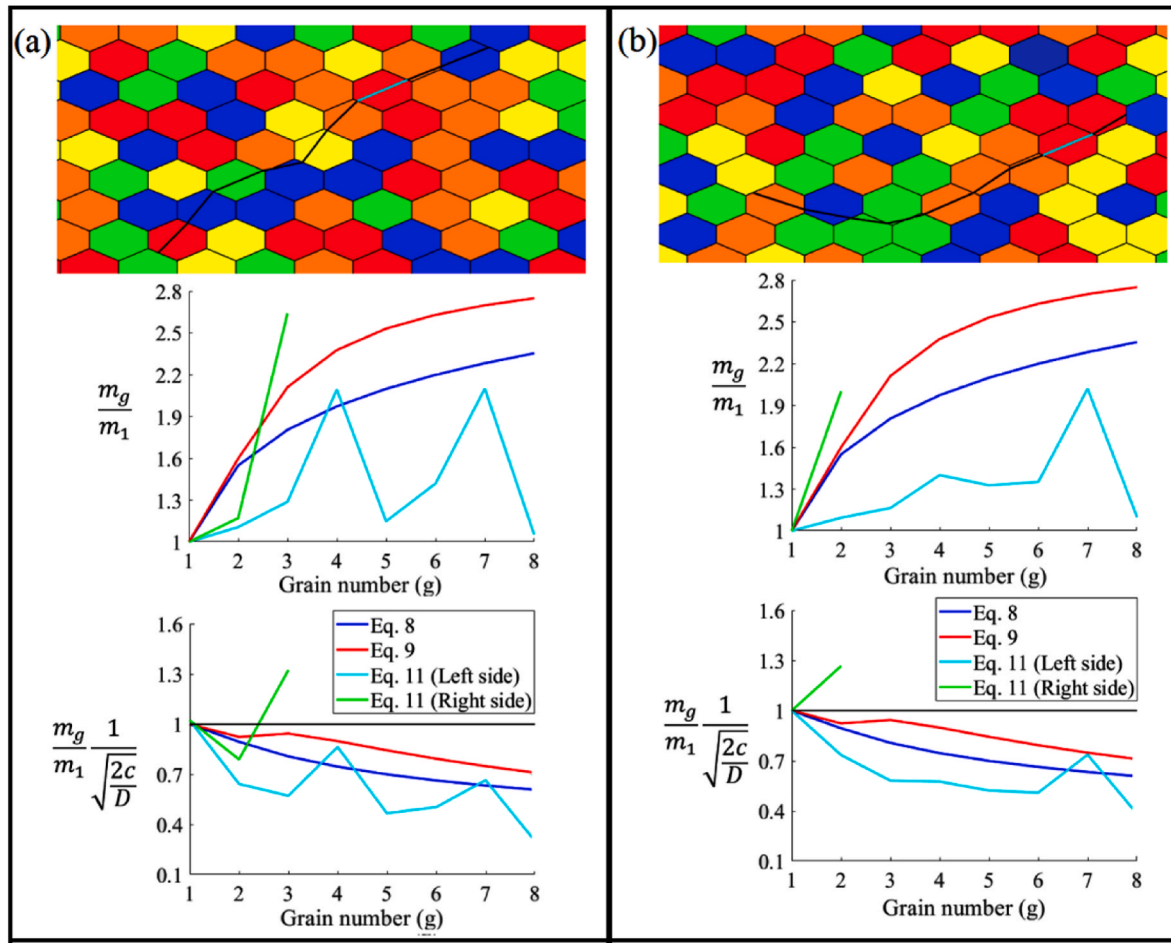


Fig. 8. Examples of cracks stopping on one side for criteria 1 and 6 a & d) crack path, b & e) evolution of grain orientation factor c & f) evolution of  $\frac{m_g}{m_1} \frac{1}{\sqrt{\frac{2c}{D}}}$ .

**Table 3**  
Results for all crack propagation criteria, including minimum number of cycles and their statistical analysis.

Criteria	Calculated Minimum Cycles ( $\times 10^3$ ) from 1000 scenarios	Fitting parameters (GEV)			(h, p) value	Estimated Minimum Cycle for $10^6$ scenarios ( $\times 10^3$ )
		$\xi$	$\mu$ ( $\times 10^3$ ) cycles	$b$ ( $\times 10^3$ ) cycles		
0	511	-0.09	512	0.677	(0, 0.85)	509
1	482	0.03	493	7.888	(0, 0.60)	473
2	501	-0.10	529	24.405	(0, 0.96)	456
3	484	-0.19	496	6.946	(0, 0.81)	472
4	452	-0.41	482	16.456	(0, 0.72)	404
5	478	-0.20	487	5.789	(0, 0.89)	467
6	478	-0.16	494	9.541	(0, 0.95)	462
7	479	-0.31	509	15.796	(0, 0.98)	445
8	486	-0.07	501	8.998	(0, 0.82)	475
9	482	-0.54	489	3.852	(0, 0.98)	467
10	485	0.12	490	3.162	(0, 0.88)	482

propagation in criteria 6, 8, 9 and 10 provides the opportunity to find other options for crack growth through the next grain instead of stopping at GB, as is the case for criteria 1, 3, 4 and 5. These alternative solutions maximize the criterion result in a higher number of cracks reaching the stage II, but higher average number of cycles is obtained for these criteria.

Statistical analysis was used to estimate the minimum number of cycles out of 1 million scenarios. The results are provided in the last column of Table 3. The difference between the worst and the best performance is from 403,847 for criterion 4 to 509,128 for criterion 0, which represent 23 % difference. Criterion 4 estimates the lowest cycles out of one million scenarios due to its low shape ( $\xi$ ) parameter. Although the location parameter of criterion 10 was smaller than most of the other criteria, it estimated the second highest number of cycles thanks to its high shape parameter, making this criterion a highly predictable one with low dispersion.

The cumulative probabilities for the one thousand scenarios of criteria 1 to 10 are shown in Fig. 9 together with the related GEV distributions and their 95 % confidence intervals. The GEV distributions (green curves) fit well the results for all criteria in agreement with the computed Anderson and Darling test reported in Table 3. For most of the criteria, the disparity between the lower and the upper bounds of the confidence intervals (blue and red curves in Fig. 9, respectively) are not significant. However, for criteria 2, 4, 6 and 7, this discrepancy is more pronounced at lower values of the cumulative probability. In particular, criterion 4 shows 95 % confidence that the minimum number of cycles spent in the MSC regime is 351,761 cycles for 1 million scenarios, a value that is 15 % lower than the 403,847 cycles predicted by the GEV distribution and 28 % lower than the one obtained out of one thousand

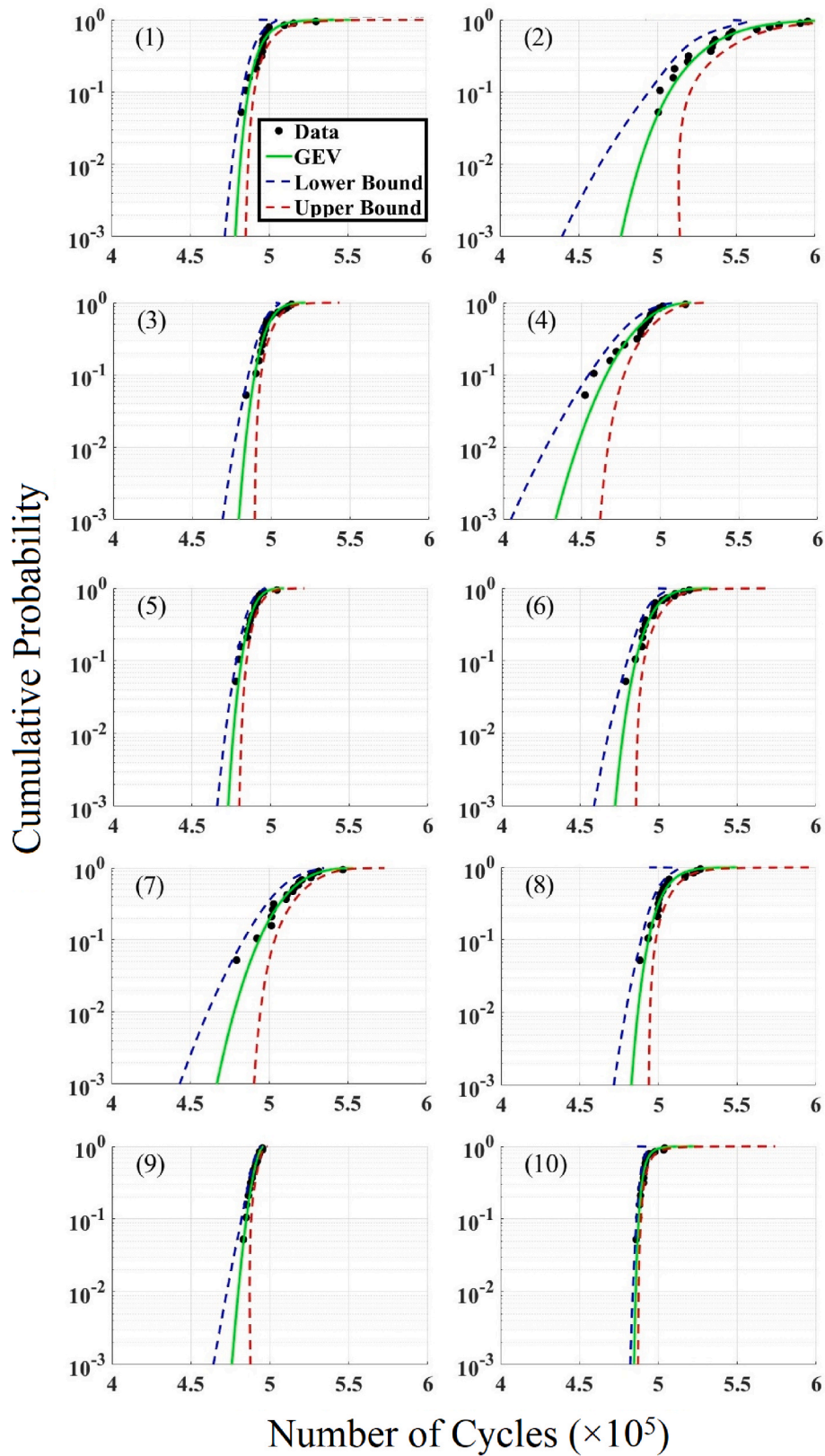


Fig. 9. GEV cumulative probability plot with 95 % confidence intervals for criteria 1 to 10.

simulations.

In order to better display the different behaviors and facilitate a comprehensive comparison of the statistical analysis in the domain of interest, Fig. 10 represents all cumulative probabilities in the same

graph and a zoom for the low probability region. All criteria, except 2, 4 and 7, display a steep curve for probabilities higher than 0.2 and the probability become approximately a vertical line in the zoomed region. In these cases, the lowest expected number of cycles spent in the MSC

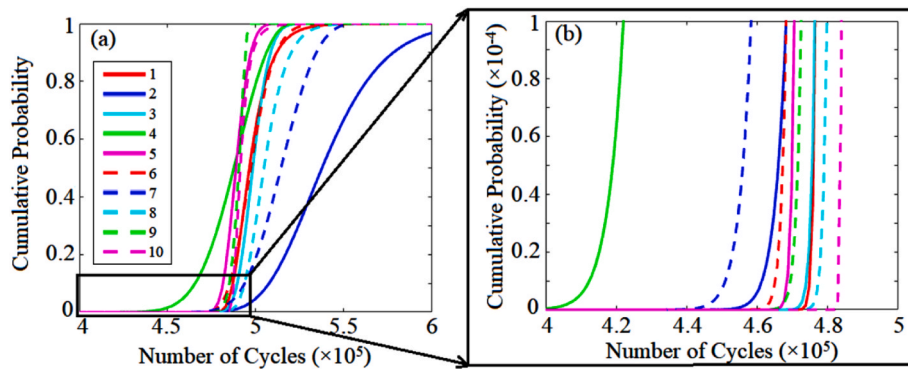


Fig. 10. GEV cumulative probability plot of all (a) all data and (b) close view of low probabilities.

regime decreases only slightly as the cumulative probability of rupture decreases, and its change is negligible when the probability is in the range of  $10^{-4}$ . In the case of criteria 2, 4 and 7, the number of cycles spent in the MSC regime keeps decreasing as the targeted cumulative probability decreases even for the cumulative probability in the range of  $10^{-4}$ .

The methodology presented above is particularly interesting as it develops the propagation criteria proposed by N-R to incorporate some features observed experimentally during the early stage of crack propagation. In the present model, the effect of GBs has been introduced in the model based on some simple propagation criteria for selecting the propagation slip system in the next grain, but more elaborate and realistic criteria should be used to fully exploit the potential of the proposed approach.

#### 4. Conclusions

Based on the Navarro and De Los Rios approach, the present investigation proposes a relatively simple model taking into account the actual properties of the grains in front of the propagating short crack. Different propagation criteria were proposed and compared and the statistical nature related to grain orientations was estimated. The dispersions in terms of the number of cycles spent in the microstructurally short crack propagation stage were calculated based on one thousand simulation and other extreme value statistics were documented. Despite its simplistic formulation in its present version, the proposed methodology was able to provide some relevant insight conclusions:

- Unlike the Navarro and De Los Rios approach, the proposed model considers the possibility for some cracks to get arrested permanently on one or both sides of a short crack. The numbers of cracks reaching to the large crack growth stage is depended on the crack propagation criteria.
- The new model gives the short crack the possibility of deflection when it reaches a grain boundary, reproducing a well-known characteristic of MSC propagation.
- The average number of cycles predicted by the presented model are around the Navarro and De Los Rios model prediction: however, the present model predicts a minimum number of cycles that can be significantly lower. Furthermore, considering the statistic nature of short-crack propagation, the new model can calculate, for a specific level of confidence, the minimum number of cycles spent in the microstructurally short crack regime.
- Based on the present version of the model, the fastest scenarios for each criterion are related to conditions for which slip systems having high Schmid factors are favored. This is due to the fact that the effect of grain boundary barriers is strongly depended on this factor in the Navarro and De Los Rios approach. Other energetic criteria will have to be tested in a more developed version of the model; in particular,

to incorporate the segmentation of a fatigue crack crossing a grain boundary, i.e. the nucleation of multiples small cracks in the next grain.

- Generalized extreme value distributions were able to describe well the obtained results on one thousand runs as supported by the calculated values of the Anderson ( $h$ ) and Darling ( $p$ ) tests.
- The possibility to consider different characteristics of microstructures in the short crack propagation model proposed by Navarro and De Los Rios gave the possibility to not only calculate the number of cycles spent in the microstructurally short crack regime but also estimate the minimum number of cycles with a defined confidence from a relatively large number of trials.
- The present statistical model will be further developed in future contributions to include more elaborate and realistic criteria based on experimental observation and geometric consideration to fully exploit its potential.

#### CRediT authorship contribution statement

**Mohammad Pourdavood:** Writing – original draft, Visualization, Software, Methodology, Investigation, Formal analysis, Conceptualization. **Philippe Bocher:** Writing – review & editing, Validation, Supervision, Project administration, Methodology, Funding acquisition, Conceptualization.

#### Declaration of competing interest

The authors declare the following financial interests/personal relationships which may be considered as potential competing interests: Mohammad Pourdavood reports financial support was provided by Natural Sciences and Engineering Research Council of Canada (NSERC).

#### Data availability

Data will be made available on request.

#### Acknowledgments

This work was financially supported by Natural Sciences and Engineering Research Council of Canada (NSERC).

#### References

- [1] H.E. Boyer, *Atlas of Fatigue Curves*, American Society for Metals, Metals Park, Ohio, 1986.
- [2] S. Lavenstein, J.A. El-Awady, Micro-scale fatigue mechanisms in metals: insights gained from small-scale experiments and discrete dislocation dynamics simulations, *Curr. Opin. Solid State Mater. Sci.* 23 (5) (2019) 100765.
- [3] P. Chowdhury, H. Sehitoglu, Mechanisms of fatigue crack growth – a critical digest of theoretical developments, *Fatig. Fract. Eng. Mater. Struct.* 39 (6) (2016) 652–674.

- [4] J.W. Pegues, M.D. Roach, N. Shamsaei, Influence of microstructure on fatigue crack nucleation and microstructurally short crack growth of an austenitic stainless steel, *Mater. Sci. Eng., A* 707 (2017) 657–667.
- [5] H.J. Christ, C.P. Fritzen, P. Köster, Micromechanical modeling of short fatigue cracks, *Curr. Opin. Solid State Mater. Sci.* 18 (4) (2014) 205–211.
- [6] G.M. Castelluccio, W.D. Musinski, D.L. McDowell, Computational micromechanics of fatigue of microstructures in the HCF–VHCF regimes, *Int. J. Fatig.* 93 (2016) 387–396.
- [7] P. Zhao, Z. Xu, M. Wang, R.D.K. Misra, G. Xie, F. Du, L. Xia, High cycle fatigue behavior and microstructure of a high-speed rail material, *Mater. Sci. Eng., A* 824 (2021) 141804.
- [8] D. Taylor, Euromech colloquium on short fatigue cracks, *Fatig. Fract. Eng. Mater. Struct.* 5 (4) (1982) 305–309.
- [9] A. Navarro, E.R. De Los Rios, A microstructurally-short fatigue crack growth equation, *Fatig. Fract. Eng. Mater. Struct.* 11 (5) (1988) 383–396.
- [10] Y.Q. Chen, S.P. Pan, M.Z. Zhou, D.Q. Yi, D.Z. Xu, Y.F. Xu, Effects of inclusions, grain boundaries and grain orientations on the fatigue crack initiation and propagation behavior of 2524-T3 Al alloy, *Mater. Sci. Eng., A* 580 (2013) 150–158.
- [11] S.A. Curtis, J.S. Romero, E.R. De Los Rios, C.A. Rodopoulos, A. Levers, Predicting the interfaces between fatigue crack growth regimes in 7150-T651 aluminium alloy using the fatigue damage map, *Mater. Sci. Eng., A* 344 (1) (2003) 79–85.
- [12] R. Bretin, M. Lévesque, P. Bocher, Neighborhood effect on the strain distribution in linearly elastic polycrystals: Part 1 – finite element study of the interaction between grains, *Int. J. Solid Struct.* 176–177 (2019) 36–48.
- [13] R. Bretin, M. Lévesque, P. Bocher, Neighborhood effect on the strain distribution in linearly elastic polycrystals: Part 2 – cellular Automaton, *Int. J. Solid Struct.* 176–177 (2019) 49–67.
- [14] D. Tang, X. He, B. Wu, L. Dang, H. Xin, Y. Li, Anisotropic fatigue performance of directed energy deposited Ti-6Al-4V: effects of build orientation, *Mater. Sci. Eng., A* 876 (2023) 145112.
- [15] S. Taira, K. Tanaka, Y. Nakai, A model of crack-tip slip band blocked by grain boundary, *Mech. Res. Commun.* 5 (6) (1978) 375–381.
- [16] E.R. De Los Rios, H.J. Mohamed, K.J. Miller, A micro-mechanics analysis for short fatigue crack growth, *Fatig. Fract. Eng. Mater. Struct.* 8 (1) (1985) 49–63.
- [17] A. Navarro, E.R. De Los Rios, Compact solution for a multizone BCS crack model with bounded or unbounded end conditions, *Philos. Mag. A* 57 (1) (1988) 43–50.
- [18] E.R. De Los Rio, A. Navarro, Considerations of grain orientation and work hardening on short-fatigue-crack modelling, *Philos. Mag. A* 61 (3) (1990) 435–449.
- [19] A. Navarro, E.R. De Los Rios, Fatigue crack growth modelling by successive blocking of dislocations, *Proc. Roy. Soc. Lond. Math. Phys. Sci.* 437 (1900) (1992) 375–390.
- [20] E.R. De Los Rios, X.J. Xin, A. Navarro, Modelling microstructurally sensitive fatigue short crack growth, *Proc. Roy. Soc. Lond. Math. Phys. Sci.* 447 (1929) (1994) 111–134.
- [21] Y. Gao, J.S. Stölken, M. Kumar, R.O. Ritchie, High-cycle fatigue of nickel-base superalloy René 104 (ME3): interaction of microstructurally small cracks with grain boundaries of known character, *Acta Mater.* 55 (9) (2007) 3155–3167.
- [22] L. Yan, J. Fan, In-situ SEM study of fatigue crack initiation and propagation behavior in 2524 aluminum alloy, *Mater. Des.* 110 (2016) 592–601.
- [23] S. Güngör, L. Edwards, Effect of surface texture on the initiation and propagation of small fatigue cracks in a forged 6082 aluminium alloy, *Mater. Sci. Eng., A* 160 (1) (1993) 17–24.
- [24] X. Ma, H. Zhai, L. Zuo, W. Zhang, S. Rui, Q. Han, J. Jiang, C. Li, G. Chen, G. Qian, Fatigue short crack propagation behavior of selective laser melted Inconel 718 alloy by in-situ SEM study: influence of orientation and temperature, *Int. J. Fatig.* 139 (2020) 105739.
- [25] A. Navarro, E.R. De Los Rios, On dimensional analysis of fatigue crack growth rate and geometrical similitude of cracks, *Fatig. Fract. Eng. Mater. Struct.* 9 (5) (1987) 373–378.
- [26] A. Navarro, E.R. De Los Rios, Short and long fatigue crack growth: a unified model, *Philos. Mag. A* 57 (1) (1988) 15–36.
- [27] T. Zhai, A.J. Wilkinson, J.W. Martin, A crystallographic mechanism for fatigue crack propagation through grain boundaries, *Acta Mater.* 48 (20) (2000) 4917–4927.
- [28] F. Foroozmehr, P. Bocher, Effect of low temperature intercritical heat-treatment on stable crack growth behavior in 13% Cr-4% Ni martensitic stainless steel multipass weldments, *Eng. Fract. Mech.* 240 (2020) 107360.
- [29] B.A. Bilby, A.H. Cottrell, K.H. Swinden, The spread of plastic yield from a notch, *Proc. Roy. Soc. Lond. Math. Phys. Sci.* 272 (1350) (1963) 304–314.
- [30] K. Hussain, E.R. De Los Rios, A. Navarro, A two-stage micromechanics model for short fatigue cracks, *Eng. Fract. Mech.* 44 (3) (1993) 425–436.
- [31] A. de Pannemaeker, S. Fouvry, J.Y. Buffiere, M. Brochu, Modelling the fretting fatigue crack growth: from short crack correction strategies to microstructural approaches, *Int. J. Fatig.* 117 (2018) 75–89.
- [32] T. Klotz, H. Miao, C. Bianchetti, M. Lévesque, M. Brochu, Analytical fatigue life prediction of shot peened Inconel 718, *Int. J. Fatig.* 113 (2018) 204–221.
- [33] L.W. Wei, E.R. De Los Rios, M.N. James, Experimental study and modelling of short fatigue crack growth in aluminium alloy Al7010-T7451 under random loading, *Int. J. Fatig.* 24 (9) (2002) 963–975.
- [34] A.J. Wilkinson, Modelling the effects of texture on the statistics of stage I fatigue crack growth, *Philos. Mag. A* 81 (4) (2001) 841–855.
- [35] W. Schaefer, M. Marx, H. Vehoff, A. Heckl, P. Randelzhofer, A 3-D view on the mechanisms of short fatigue cracks interacting with grain boundaries, *Acta Mater.* 59 (5) (2011) 1849–1861.
- [36] F. Briffod, A. Bleuset, T. Shiraiwa, M. Enoki, Effect of crystallographic orientation and geometrical compatibility on fatigue crack initiation and propagation in rolled Ti-6Al-4V alloy, *Acta Mater.* 177 (2019) 56–67.
- [37] M. Ma, B. Wang, H. Liu, D. Yi, F. Shen, T. Zhai, Investigation of fatigue crack propagation behavior of 5083 aluminum alloy under various stress ratios: role of grain boundary and Schmid factor, *Mater. Sci. Eng., A* 773 (2020) 138871.
- [38] J. Luster, M. Morris, Compatibility of deformation in two-phase Ti-Al alloys: dependence on microstructure and orientation relationships, *Metall. Mater. Trans.* 26 (7) (1995) 1745–1756.
- [39] T.W. Anderson, D.A. Darling, A test of goodness of fit, *J. Am. Stat. Assoc.* 49 (268) (1954) 765–769.
- [40] L. Tello, L. Castejon, H. Malon, D. Valladares, P. Luque, D.A. Mantaras, D. Ranz, J. Cuartero, Development of a fatigue life prediction methodology for welded steel semi-trailer components based on a new criterion, *Eng. Fail. Anal.* 108 (2020) 104268.
- [41] A. Bag, D. Delbergue, J. Ajaja, P. Bocher, M. Lévesque, M. Brochu, Effect of different shot peening conditions on the fatigue life of 300 M steel submitted to high stress amplitudes, *Int. J. Fatig.* 130 (2020) 105274.
- [42] S. Coles, J. Bawa, L. Trenner, P. Dorazio, *An Introduction to Statistical Modeling of Extreme Values*, Springer, 2001.
- [43] H. Javadi, W. Jomaa, E. Dalgaard, M. Brochu, P. Bocher, Influence of Surface Residual Stresses on the Fatigue Life and Crack Propagation Behavior of Turned Inconel 718 Super-alloy, *MATEC Web of Conferences*, EDP Sciences, 2018 18004.